Comparing Signal-to-Noise Ratio for Prostate Imaging at 7T and 3T

Bart R. Steensma, MSc,[1*] Mariska Luttje, MD, PhD,[1] Ingmar J. Voogt,[1] Dennis W.J. Klomp, PhD,[1] Professor Peter R. Luijten,[1] Cornelis A.T. van den Berg, PhD,[2] and Alexander J.E. Raaijmakers, PhD[1,3]

Background: In MRI, the signal-to-noise ratio (SNR) theoretically increases with B_0 field strength. However, because of attenuation of the radiofrequency (RF) fields at 7T, it is not certain if this SNR gain can be realized for prostate imaging.
Purpose/Hypothesis: To investigate the SNR gain in prostate imaging at 7T as compared with 3T. It is expected that SNR will improve for prostate imaging at 7T compared with 3T.
Study Type: Prospective.
Subjects: Four healthy volunteers and one prostate cancer patient.
Field Strength/Sequence: All subjects were scanned at 3T and at 7T using optimal coil setups for both field strengths. For all volunteers, proton density-weighted images were acquired for SNR analysis and actual flip angle imaging (AFI) $B_1^{+|}$ maps were acquired for correction of measured SNR values. In the patient, a T_2-weighted (T_2w) image was acquired at 3T and at 7T.
Assessment: SNR was calculated in the prostate region for all volunteers. SNR was normalized for flip angle, receiver bandwidth, and voxel volume. SNR was also calculated for different sensitivity encoding (SENSE) acceleration factors.
Statistical Testing: SNR values are represented as the arithmetic mean of SNR values in the prostate. Estimated SNR in the T_2w image is calculated as the arithmetic mean of the signal intensity (SI) divided by the standard deviation of the SI in a specified zone. Tumor-to-tissue contrast is calculated as $(SI_{tumor}+SI_{zone})/(SI_{tumor}-SI_{zone})$.
Results: An increase in SNR ranging from 1.7-fold to 2.8-fold was measured in the prostate at 7T in comparison to 3T for four volunteers. At 7T, it is possible to achieve a 4-fold SENSE acceleration in the left-right direction with similar SNR to a nonaccelerated 3T image. T_2w imaging was done at 3T and 7T in one patient, where improved tumor-to-tissue contrast was demonstrated at 7T.
Data Conclusion: SNR improves for prostate imaging at 7T as compared with 3T.
Level of Evidence: 2
Technical Efficacy: Stage 1

J. MAGN. RESON. IMAGING 2019;49:1446–1455.

PROSTATE CANCER is one of the most common forms of cancer in men, affecting one out of six men during their lifetime.[1] Prostate cancer is often indolent and could be followed up by a watchful-waiting program when noninvasive imaging/characterization methods are available. Therefore, it is necessary to improve noninvasive tumor characterization methods for selective treatment of only those tumors that are potentially harmful and which have extracapsular extension.[2]

Multiple studies have shown that multiparametric prostate magnetic resonance imaging (MRI) at 1.5 and 3T is helpful in detecting, localizing, and staging prostate cancer; however, so far good correlation with disease aggressiveness is insufficient to prevent potentially unnecessary treatment.[3–7] More insight into tumor metabolism and aggressiveness could be obtained by using MR spectroscopy (MRS)[8–10] and higher-resolution imaging for capsular extension,[11] but for better results a higher signal-to-noise ratio (SNR) is needed.

View this article online at wileyonlinelibrary.com. DOI: 10.1002/jmri.26527

Received Jun 17, 2018, Accepted for publication Sep 12, 2018.

*Address reprint requests to: B.R.S.,, Heidelberglaan 100 3584 CX, Utrecht, The Netherlands. E-mail: b.r.steensma@umcutrecht.nl

From the [1]University Medical Center Utrecht, Department of Radiology, Utrecht, The Netherlands; [2]University Medical Center Utrecht, Department of Radiotherapy, Utrecht, The Netherlands; and [3]Eindhoven University of Technology, Department of Biomedical Engineering, Utrecht, The Netherlands

Additional supporting information may be found in the online version of this article.

The SNR for prostate MRI increases by going from 1.5 to 3T,[12] and a further increase is expected when going to 7T systems. A recent study[13] compared 7T abdominal imaging to 1.5T and 3T, but focused mainly on image quality and did not show results for prostate imaging.

Patient studies at 7T involving prostate cancer showed until now satisfactory results for T_2w (T_2-weighted) imaging compared with 3T[14] and the first results of ^{1}H and ^{31}P MRS[15–17] at 7T were published. Imaging at 7T is technically challenging due to radiofrequency (RF) inhomogeneity, increased tissue heating, and reduced RF field penetration. These challenges could potentially diminish the advantages of 7T. Although numerous studies have documented the use of custom-built external arrays dedicated to prostate imaging at 7T to obtain good T_2w imaging,[18–22] until now the superior imaging performance of 7T over 3T has not been demonstrated in terms of SNR. This, combined with the increased RF field attenuation at 7T, casts doubts on whether or not imaging of deeply located structures within the body such as the prostate will actually be beneficial at 7T.

SNR comparisons over field strengths are challenging, as they depend on a wide range of parameters. Relaxation time constants are different, causing sequence parameters like echo time (TE) and repetition time (TR) optimized for one field strength to be different for the other field strength. Moreover, the RF coil arrays that can be used will be different, and even if an identical coil geometry is used, the electromagnetic interaction with the body is completely different, causing an optimized array for one field to be suboptimal for the other. Next, the uniformity of excitation will be different between field strengths, causing inhomogeneous flip angles, tissue contrast, and SNR. Finally, the specific absorption rate (SAR) may prohibit the use of optimized sequence parameters, which can result in suboptimal scan efficiencies and thus SNR penalties.

One of the ways to minimize the number of parameters in comparing SNR over field strengths is to assess the SNR for a proton density-weighted acquisition at a high flip angle.[23–25] An image acquisition with a 90° flip angle, very short echo time, and large TR can negate the effect of relaxation parameters and RF transmit uniformity differences between field strengths. The long TR acquisition will not be limited by SAR constraints, and so can be applied uncompromised at all field strengths. Based on the individual multichannel images, coil sensitivity data, and noise prescan data, SNR scaled images can be reconstructed.[26,27] These SNR scaled images can be corrected with a flip angle map, the receiver bandwidth, and the voxel size to provide a measure for the SNR that actually can be obtained with each system, independent of scan parameters and tissue relaxation times. This is referred to as system SNR. Further corrections with quality factor ratio and preamplifier noise figure are needed to assess what is called intrinsic SNR,[23] which is the SNR at a system corrected for potential system imperfections. Because of difficulties in determining the Q-factor ratios for commercial arrays, the intrinsic SNR can only be determined by estimates of this ratio, with accompanying uncertainties. This is discussed in more detail in the Discussion section. Also, because the choice of going from one field strength to the other is determined by the system SNR, this study will focus predominantly on a system SNR comparison.

A higher SNR is not the only gain at 7T; also parallel imaging performance is expected to improve when moving from 3T to 7T because of the more distinct sensitivity profiles of individual coil elements at 7T.[28] Based on the multichannel images and sensitivity data, g-factor maps, and SNR scaled images can be compared at different sensitivity encoding (SENSE) acceleration factors, to compare parallel imaging performance at 3T and 7T.

The purpose of this work was to investigate the SNR gain in prostate imaging at 7T as compared with 3T. It is demonstrated in four volunteers and a phantom that SNR improves more than twofold in the prostate. SNR performance is also compared for different acceleration factors in the left-right (LR) direction. To demonstrate utilization of the enhanced SNR at 7T, T_2w images were acquired in one patient with prostate cancer.

Materials and Methods

This study was approved by the Institutional Review Board and informed consent from all subjects was obtained.

Coil Configuration and Setup

For this study an 8-element transceiver array consisting of fractionated dipole antennas[21] was combined with a detunable 16-element receive only loop coil array,[29] Fig. 1. Eight building blocks consisting of one transceive dipole and two receive loops were distributed over the pelvis as indicated in Fig. 1, with four columns of receive elements distributed in the LR direction. Under each antenna two oval-shaped receive loops (long axis: 16 cm, short axis 10 cm) were positioned with mutual overlap. The antenna length was 30 cm with two meanders distributed evenly in each leg. The receive coil dimensions are based on the dipole size as well as the circumference of an average European adult, for which a certain optimal loop size exists.[30] The antenna was placed at a distance of 2 cm from the body. To reduce coupling of the receive loops to the antenna, while ensuring sufficient coupling to the human body, a body-loop distance of 6 mm was found for the optimal $Q_{unloaded}/Q_{loaded}$ ratio (140/11). Detuning networks block the current inside the loops at three locations during transmit. A lattice balun was used to suppress common mode currents. Preamp decoupling was implemented to reduce interelement coupling. Simultaneously, the preamp decoupling network in each receive loop (where the cable is connected) acts as a high impedance for induced currents in the loop, which in addition to detuning contributes to suppressing induced currents in the loop during transmit. More details on the tuning and matching circuitry and the RF safety profile of this coil array were provided

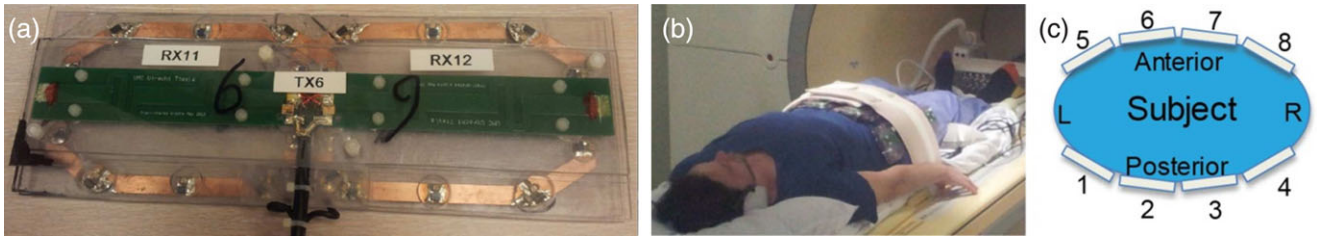

FIGURE 1: Experimental setup: (a) Under each antenna two oval-shaped receive loops were positioned. To ensure spacing from the antenna towards the patient, a 20-mm polycarbonate placeholder was designed in which the loops were at 6 mm distance from the patient. (b,c) The 8-element array with receive loops was positioned in a belt-like fashion around the pelvis.

previously.[29] Each antenna / two loop structure was one of eight separate elements that were placed around the pelvis.

To ensure RF safety, a conservative worst-case SAR scenario was assumed,[31] resulting in average power limits of 4W per channel to achieve the 20W/kg SAR limit of the IEC guidelines for any phase setting. The described array was interfaced using an 8-channel transmit/receive switch and receive interface box (MR Coils, Zaltbommel, The Netherlands) to an Achieva 7T MR system (Philips Healthcare, Best, The Netherlands). The 3T results were acquired on a Philips Ingenia 3T system (Philips Healthcare), using the commercially available anterior and posterior body array with up to 32 elements (Philips Healthcare), with four columns of receive loops distributed in the LR direction.

MRI Acquisition Volunteers and Phantom

Four healthy volunteers (ages 29, 44, 38, and 33, BMI 25.5, 25.5, 23.6, and 27.1 kg/m^2 were included in this study. The MRI protocol for healthy volunteers included the following exams at 3T and 7T: A survey for localization purposes, a dynamic series of spoiled gradient echoes with alternating active transmit channels (shim series, only at 7T) to calibrate B_1 levels in the prostate,[32] AFI B_1 map,[33] T_2w imaging for anatomical images, and a proton density-weighted gradient echo acquisition for SNR comparison. Based on the shim series, relative phase maps could be derived for every transmit channel. Optimal transmit phases that maximize average $B_1^{+|}$ in the prostate were determined for every transmit channel using a minimization procedure in MatLab (MathWorks, Natick, MA). Noise levels were determined using a noise prescan, which was acquired without RF or gradients. The proton density-weighted gradient echo sequence (SNR scan) was obtained using TR/TE = 10,000/5 msec, flip angle = 90°, field of view (FOV) = 320 × 440 × 44 mm^3, voxel size = 5 × 10 × 10 mm^3, receive bandwidth = 1011 Hz, nominal $B_1^{+|}$ 12 μT, pulse width = 3.866 msec, acquisition time = 1305 sec. The TE was kept short to exclude T_2 effects, while for T_1 exclusion the TR was kept long. A flip angle of 90° was used to be relatively insensitive to transmit nonuniformities. The actual flip angle method[33] was used for $B_1^{+|}$-mapping, using the following scan parameters: 3D fast-field echo (FFE) sequence, TR/TE = 50/2.6 msec. TR extension = 200 msec, flip angle = 65°, FOV = 250 × 422 × 50 mm^3, resolution = 3.9 × 3.8 × 10 mm^3. Receive bandwidth = 257 Hz (7T) and 110 Hz (3T), nominal $B_1^{+|}$ = 11.8 μT (7T) and 13.46 μT (3T), pulse width = 2.99 msec (7T), 2.48 msec (3T), acquisition time 105 sec. All experiments were repeated on a phantom with electric properties and dimensions comparable to the human pelvis (ethylene glycol, 50 g NaCl/L, ε_r = 34, σ = 0.4 S/m, width = 390 mm, height = 190 mm, length = 370 mm).

MRI Acquisition Patient

One patient (62 years, prostate specific antigen [PSA]: 9.7 ng/ml) with biopsy-proven prostate cancer (Gleason score: 3 + 4 in 9/10 biopsies) was included in this study. A clinical prostate MRI exam was performed at 3T using a 32-element torso/cardiac coil (Philips Ingenia). The T_2w acquisition was acquired using the following parameters: TR/TE = 5900/100 msec, turbo spin echo (TSE) factor = 29, SENSE factor RL = 1.5, FOV = 200 × 200 × 90 mm^3, voxel size = 0.78 × 0.78 × 3 mm^3, and reconstruction voxel size = 0.5 × 0.5 × 3 mm^3.

At 7T the protocol consisted of a survey for localization purposes, B_1 shim series to optimize B_1 levels in the prostate,[32] AFI B_1 map,[33] and one single slice T_2w sequence (TR/TE = 2500/90 msec) with the same voxel dimensions as the clinical sequence at 3T. In addition, this sequence has been repeated with higher resolutions (voxel size: 0.5 × 0.5 × 4 mm^3, 0.5 × 0.5 × 2 mm^3, 0.35 × 0.35 × 4 mm^3, and 0.35 × 0.35 × 2 mm^3) to explore the possibilities that the extra SNR provides. Scan parameters for all sequences are listed in Table 1.

At both field strengths and all resolutions, estimated SNR (eSNR) was assessed in the peripheral zone (PZ), the central gland, and in the two indicated tumor regions by calculating the mean signal intensity (SI) divided by the standard deviation of the SI.[34] Contrast between the tumor and the zone in which the tumor was located was calculated as $(SI_{tumor}+SI_{zone})/(SI_{tumor}-SI_{zone})$.

SNR Analysis

Complex image data, coil sensitivity data, and noise data were acquired for every channel and exported using ReconFrame (Gyrotools, Switzerland). The method of Kellman and McVeigh[26,35] was used to obtain SNR scaled images, using the following steps. A noise-covariance matrix R with dimension (N_{ch} × N_{ch}) was calculated from the prescan noise data. R was corrected for the bandwidth of the digital receiver using a bandwidth correction factor of B_c = 0.73, which was calculated based on measuring the noise equivalent bandwidth in the noise data for both setups as described in Kellman and McVeigh.[26] The noise covariance data R was then scaled as $R_{corrected} = R/B_c$. The lower triangular Cholesky product L of the noise covariance matrix ($L^{-1}L = R$) was calculated for noise prewhitening. A noise prewhitening step was applied to the sensitivity data b and the image data p (both vectors of length N_{ch}) for every voxel:

TABLE 1. Scan Parameters of All Sequences for 3T and 7T

Sequence	PD Weighted image (3T/7T)	AFI B1map (3T/7T)	T2w (3T)	T2w (7T)	T2w (7T)	T2w (7T)
Sequence type	M2D FFE	3D FFE	M2D TSE	2D TSE		
TR	10000 msec	50 ms, 200 msec TR extension	5900 msec	2500 msec		
TE	5 msec	2.6 msec	100 msec	90 msec		
Flip angle	90°	65°	90°/180° refocusing pulse	90°/180° refocusing pulse		
FOV	320 × 440 × 44 mm^3	240 × 422 × 50 mm^3	200 × 200 × 90 mm^3	200 × 200 × 3 mm^3		
Voxel size	5 × 10 × 10 mm^3	3.9 × 3.8 × 10 mm^3	0.78 × 0.78 × 3 mm^3	0.78 × 0.78 × 3 mm^3	0.5 × 0.5 × 3 mm^3	0.35 × 0.35 × 3 mm^3
Slices	3	5	30	1		
TSE factor	—	—	29	17		
Acquisition time	1305 sec	105 sec	176 sec	25 sec	39 sec	56 sec
Receive bandwidth	1011 Hz	110 Hz (3T) and 257 Hz (7T)	—	—	—	—
Nominal B1	12 μT	13.46 μT (3T) and 11.8 μT (7T)	—	—	—	—
Pulse width	3.866 msec	2.48 ms (3T) and 2.99 msec (7T)	—	—	—	—
Acceleration factor	R=1	R=1	R=1.5	R=1.5		

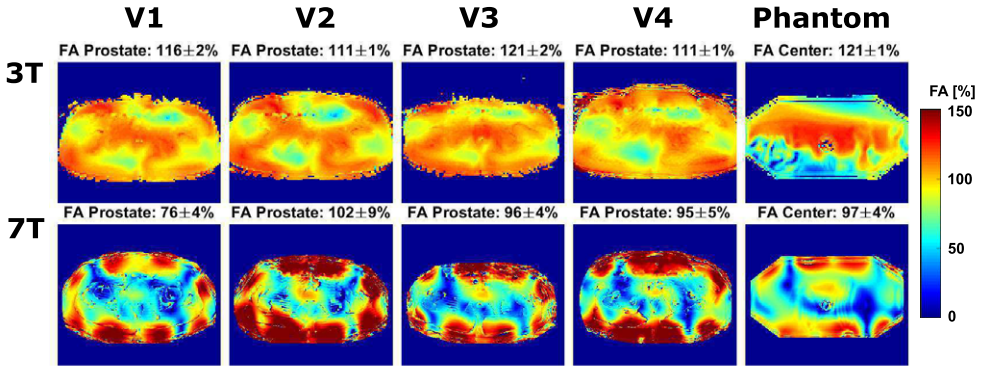

FIGURE 2: Flip angle maps in four volunteers and a phantom at 3T and 7T. B_1 inhomogeneities are clearly present throughout the image at 7T. Signal voids are also present at 3T, but less severe. The flip angle seems lower at the edges of the phantom at 3T due to the limited dynamic range of the AFI-method.

$$\tilde{p} = pL, \tilde{b} = bL \tag{1}$$

The noise prewhitening step ensures that standard deviation of the noise is uniform for every channel in the reconstructed image. Sensitivity-weighted reconstruction with SNR scaling was done following the approach of Roemer et al[35]:

$$\mathrm{SNR}_{pixel} = \sqrt{2}|\tilde{b}^T\tilde{p}|/\sqrt{(\tilde{b}^T b)} \tag{2}$$

The reconstructed image provides a quantitative map in which the value in every voxel represents the local SNR. This SNR is indicated as pixel SNR. For each SNR image a rectangular region of interest (ROI, 10 × 10 voxels) was delineated within the prostate, after which the measured SNR could be determined as the mean signal level in the ROI. The SNR images consisted of three slices, of which only the middle slice was considered, to avoid intravoxel dephasing due to slice profile imperfections. The pixel SNR still is potentially biased by differences in scan parameters and transmit efficiency. Therefore, the pixel SNR was corrected based on receive bandwidth (BW_R), voxel volume (V), average flip angle in the prostate (θ_p) according to the following formula[23] to result in the system SNR:

$$SNR_{system} = SNR_{pixel}\frac{\sqrt{BW_R}}{V\sin(\theta_p)} \tag{3}$$

Further corrections are possible to remove system imperfections from the equation. These imperfections can be characterized by the system noise figure (NF) and the loaded to unloaded quality-factor (Q-factor) ratio. The result is the so-called intrinsic SNR:

$$SNR_{intrinstic} = SNR_{system}\frac{10^{\frac{NF}{20}}}{\left[1-\frac{Q_{loaded}}{Q_{unloaded}}\right]^{\frac{1}{2}}} \tag{4}$$

The preamplifier noise figures were measured using a Hewlett-Packard 8970A Noise Figure Meter (Palo Alto, CA). The Q-factors of the loops at 7T were measured using a sniffer coil.[36] The Q-factor of the dipole antennas was measured using the recently published method of Chen et al.[37] The Q-factors of the commercial loop array at 3T could not be measured.

Parallel Imaging Performance

The coil sensitivity data and image data were also used for assessment of parallel imaging performance. Image data was undersampled in *k*-space, after which a geometry-factor (g-factor) map was calculated using SENSE reconstruction.[38] SNR for the accelerated images was calculated as:

$$SNR_{accelerated} = \frac{SNR_{unaccelerated}}{g\sqrt{R}} \tag{5}$$

For this work, undersampling was applied only in the LR direction. This corresponds to the phase-encoding direction that is normally used in 2D T_2w-acquitisions at this site, to avoid folding artifacts of the iliac arteries in the prostate region. For one volunteer at 7T, a multislice T_2w image (18 slices) was acquired using the same scan parameters used by Maas et al,[19] with an acceleration factor of R = 2 and R = 4 in the LR direction.

Results

Coil Array Characterization

The preamplifier noise figure was 0.56 dB at 3T and 0.78 dB at 7T. The unloaded to loaded Q-ratio at 7T was 13 for the loops and 11 for the dipole antennas. Noise correlation between coil array elements can potentially decrease the SNR in MRI. The noise correlation matrix of an array is therefore one of the indicators of an array's imaging performance. The noise correlation matrix was obtained for each volunteer at both 3T and 7T. A typical example of a matrix is added as Supporting Information (Fig. S1). Noticeable is that the coupling between elements, particularly within the posterior part of the coil array at 3T, is higher compared with any coupling between elements at 7T.

Flip Angle Maps

Figure 2 shows the relative flip angle distributions in the phantom and in four volunteers.

It is clearly visible that at 7T, the penetration depth of the RF transmit fields is decreased and B_1 inhomogeneities are present throughout the pelvis. At 3T, three distinct

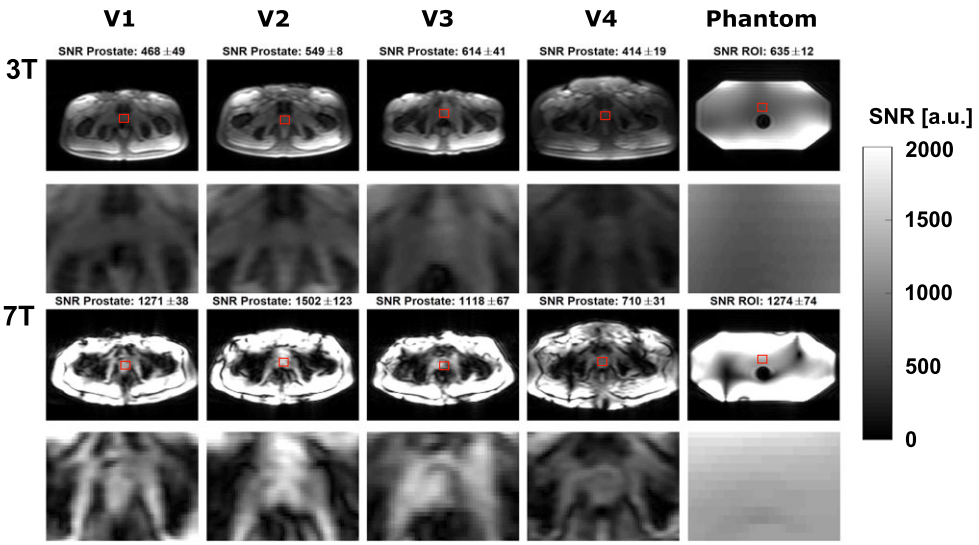

FIGURE 3: SNR scaled images on four volunteers and a phantom for 3T and 7T. The first and third rows show the full image, while the second and fourth rows show a cropped image centered around the prostate. SNR was calculated in the indicated red ROI, which is located within the prostate for all volunteers. The SNR values in this figure are pixel SNR values, and are not yet corrected for scan parameters.

regions of lower B_1 are present in all volunteers, showing that B_1 inhomogeneities are also present at 3T; however, clearly less severe than at 7T. At 7T, the flip angle distribution is less uniform than at 3T (coefficient of variation 44.4% at 7T and 16.6% at 3T), this difference is caused by the shorter wavelength and interference effects at 7T. Above each figure, the average and standard deviation of the flip angle in the ROI is shown. The average relative flip angle in the prostate is 93.2% at 7T and 116% at 3T. The large flip angle at 3T is because the RF power calibration tries to optimize the flip angle over the whole FOV, which also contains many regions where the flip angle is lower than 100% (Fig. 3). The standard deviation of the flip angle in the prostate is 5.2% at 7T and 1.4% at 3T. At 7T, an average peak input power of 8*622.7W and a 2.989 msec Gaussian pulse were used. At 3T, an average peak input power of 5008W (channel 1) and 9891W (channel 2) and a Gaussian pulse of 2.483 msec were used.

SNR

Pixel SNR maps are shown in Fig. 3. For all scans, SNR in the prostate increases when going from 3T to 7T. The SNR at 7T is especially very high close to the coil, which is less visible at 3T.

The average flip angles in the prostate, the readout bandwidth (1011 Hz), and the voxel volume were used to normalize SNR values in the prostate to system SNR values. These values are shown in Fig. 4. Average SNR in the prostate increases from (3.4, max 4.1, min 2.7)*10^4 √Hz/ml at 3T to (7.5, max 9.5, min 4.5)*10^4 √Hz/ml at 7T, which corresponds to a minimum increase of 1.7-fold and a maximum increase of 2.8-fold. The SNR in the phantom is 4.3*10^4 √Hz/ml at 3T and 8.1*10^4 √Hz/ml at 7T.

Parallel Imaging Performance

Figure 5 shows g-factor maps (two top rows) and SNR scaled images (two bottom rows) for 3T and 7T. At 3T, g-factors above 2 start appearing in the image at acceleration factor R = 3, while at 7T acceleration factors up to R = 5 can be applied before g-factors above 2 appear. As a result of this, SNR values degrade more strongly for high acceleration factors (starting from R = 3) at 3T as compared with 7T.

Figure 6 shows the normalized SNR values in the prostate, for different acceleration factors and averaged over all

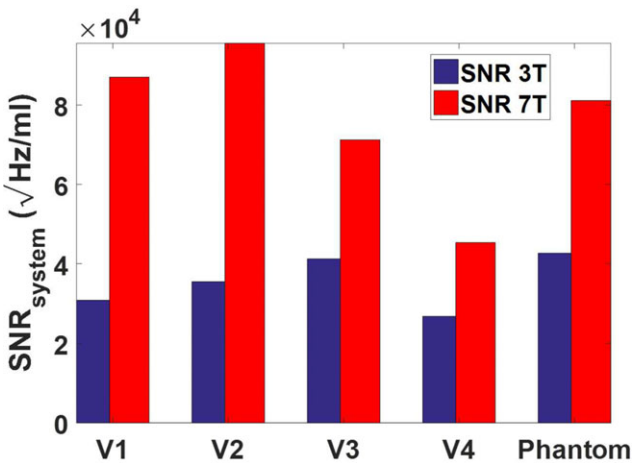

SNR [10^4 $Hz^{1/2}ml^{-1}$]	V1	V2	V3	V4	Phantom
3T	3.1	3.5	4.1	2.7	4.3
7T	8.7	9.6	7.1	4.5	8.1

FIGURE 4: System SNR values were obtained by normalizing the average pixel SNR values in the prostate to readout bandwidth, voxel size, and flip angle. At 3T, an average SNR value of 3.4e4 ± 0.6e4 √Hz/ml was measured. At 7T, this value increased to 7.5e4 ± 2.2e4 √Hz/ml, which corresponds to a 2.2-fold increase.

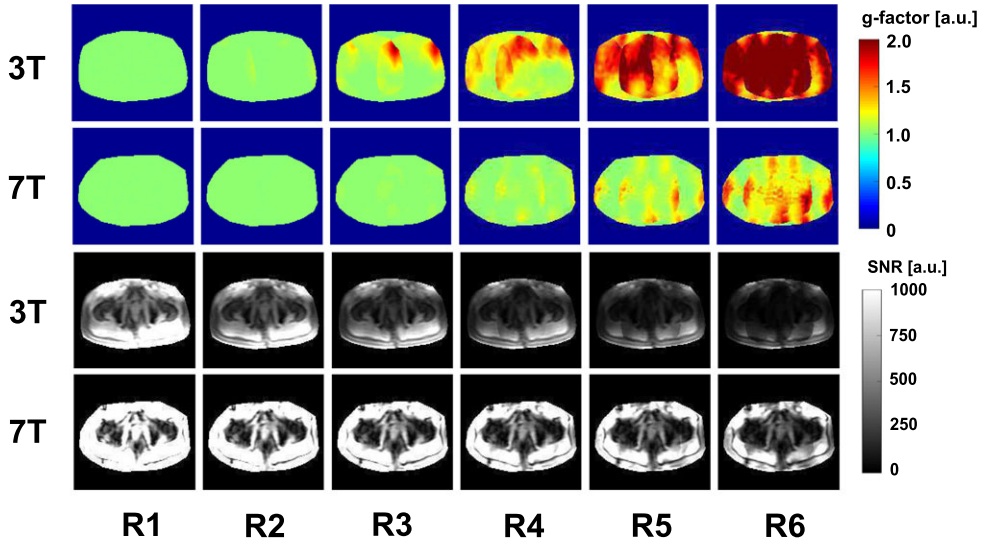

FIGURE 5: g-factor maps (two top rows) and pixel SNR values (two bottom rows) for 3T and 7T using different LR-acceleration factors in an exemplary volunteer (V1). The pixel SNR maps are not yet corrected to system SNR values.

volunteers. Because of the improved parallel imaging performance and the improved SNR at 7T, an acceleration factor of R = 4 can be applied at 7T with SNR, comparable to an unaccelerated 3T prostate image. A multislice T_2 image of a volunteer acquired with LR acceleration factor R = 2 and R = 4 is shown in the Supporting Information (Fig. S1). eSNR decreases from 12.3 to 10.8 when increasing the acceleration factor.

T_2w Imaging

In one prostate cancer patient (62 years, PSA: 9.7 ng/ml, Gleason score: 3 + 4), T_2w images were acquired at 7T after the clinical 3T MR examination. Figure 7 shows a close-up view of the prostate at both field strengths.

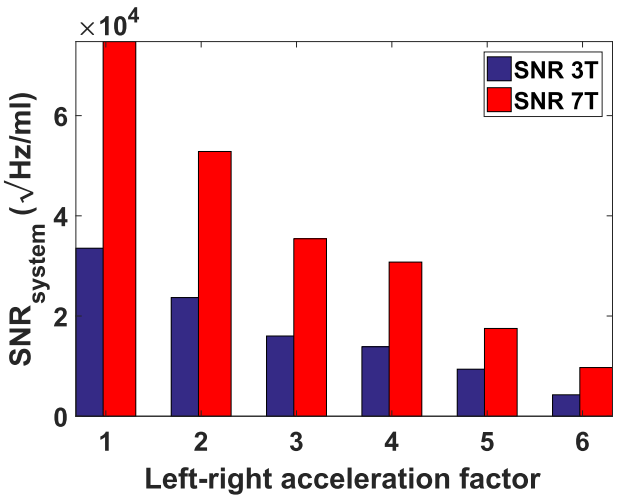

SNR [10^4 $Hz^{1/2}ml^{-1}$]	R=1	R=2	R=3	R=4	R=5	R=6
3T	3.4	2.4	1.6	1.4	0.9	0.4
7T	7.5	5.3	3.5	3.1	1.8	1.0

FIGURE 6: System SNR values in the prostate for 3T and 7T for different LR-acceleration factors, averaged over all four volunteers.

Table 2 shows eSNR and contrast values in the T_2w images at 3T and 7T.

eSNR values differ per region and per field strength, but a correlation between eSNR and field strength cannot be seen. When increasing the resolution, eSNR generally decreases. For the tumor area in the central gland, the contrast improves from 0.09 at 3T to 0.19 at 7T. For the tumor area in the peripheral zone, contrast improves from 0.08 at 3T to 0.15 at 7T. When increasing the resolution from 0.78 × 0.78 × 3 mm^3 to 0.5 × 0.5 × 2 mm^3 at 7T, tumor-to-TZ contrast improves from 0.19 to 0.31, while tumor-to-PZ contrast remains the same. When further increasing the resolution to 0.35 × 0.35 × 2 mm, tumor-to-TZ contrast decreases again from 0.31 to 0.20, while tumor-to-PZ contrast decreases from 0.15 to 0.09. Figure 8 shows T_2w images at 7T for increasing resolution.

Discussion

In this work we demonstrated an increase in SNR for prostate MRI at 7T in comparison to 3T, which ranges from 1.7-fold to 2.8-fold. No direct relationship between BMI and SNR can be observed, except that the subject with the highest BMI shows the lowest SNR at both field strengths and also the lowest SNR gain at 7T. This is potentially related to the decreased penetration depth of the RF fields at 7T. The SNR values reported in this work are comparable to the SNR values reported by Erturk et al with a 16-channel loop-dipole array[39] (7.2e4 ± 1.0e4 √Hz/ml in Erturk et al vs. 7.5e4 ± 2.4 e4 √Hz/ml in this work).

Parallel imaging performance was also evaluated for 7T and 3T. At 7T, higher acceleration factors can be applied (R = 5) as compared with 3T (R = 3) before g-factors in the imaging region exceed the value of 2. The enhanced parallel

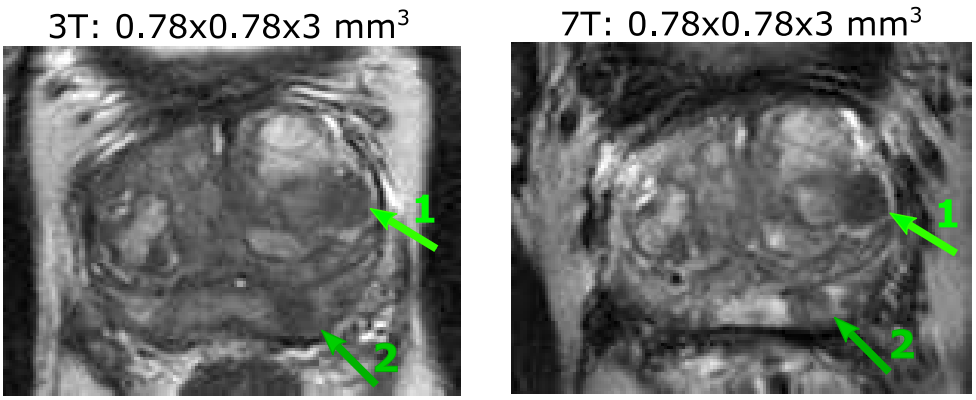

FIGURE 7: In this patient (62 years, PSA: 9.7 ng/ml) with biopsy-proven prostate cancer (Gleason score: 3 + 4 in 9/10 biopsies), two tumor areas are visible mid-prostate. Area 1 indicates a tumor region in the central gland, area 2 indicates a tumor region in the peripheral zone.

TABLE 2. Estimated SNR and Contrast Values in the Central Gland, the Peripheral Zone (PZ), and Both Tumor Regions for One Prostate Patient

Field strength	Voxel size	Gland eSNR	Gland tumor eSNR	Tumor-to-gland contrast	PZ eSNR	PZ tumor eSNR	Tumor-to-PZ contrast
3T	0.78x0.78x3 mm^3	3.4	4.1	0.09	4.5	6.2	0.08
7T	0.78x0.78x3 mm^3	4.2	3.0	0.19	3.5	4.1	0.15
7T	0.5x0.5x2 mm^3	3.5	2.9	0.31	3.2	3.4	0.15
7T	0.35x0.35x2 mm^3	3.4	2.6	0.2	3.1	4.0	0.09

imaging performance with increasing field strength corresponds to predictions based on an analytical model.[28] The high SNR and low g-factor at 7T enable 4-fold acceleration with comparable SNR to an unaccelerated 3T image. (SNR at 7T 3.1e4 √Hz/ml at R = 4, SNR at 3T: 3.4e4 √Hz/ml at R = 1). This effectively means that the g-factor with R = 4 is almost entirely equal to 1, so the loss in SNR from acceleration is determined by the square root of the acceleration factor. This loss for R = 4 is equal to 2, which is then compensated by the SNR gain at 7T.

The improved parallel imaging performance at 7T can be used to accelerate clinical protocols as compared with 3T, making it possible to acquire 4-fold more slices in the same amount of time and with similar SNR. However, this is only possible if SAR limitations are not exceeded, which can be a problem for clinical protocols at 7T. The T_2w images in this study were acquired with only one slice to avoid any SAR violations. Additional measures have been published to further reduce SAR levels for T_2w prostate imaging at 7T, which made it possible to acquire clinical T_2w images at 7T.[19] The

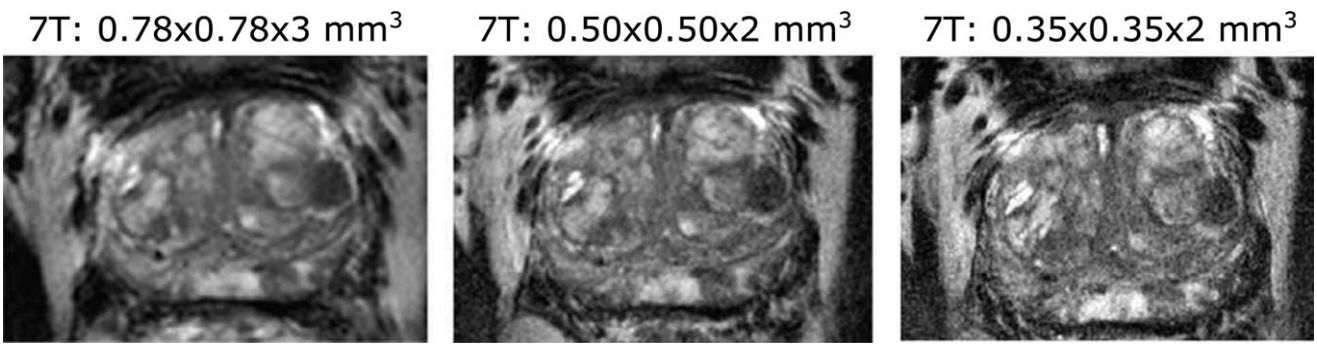

FIGURE 8: T_2w images acquired at 7T with increased resolution. Anatomical details and contrast between healthy and tumor areas remain visible even at the resolution of 0.35 × 0.35 × 2 mm^3.

potential for using higher parallel imaging factors might also be used to reduce SAR load in the TSE sequence.

Comparing the clinical T_2w images at 3T and 7T shows that the same anatomical information is present at both field strengths. Using the SNR gain at 7T, we acquired T_2w images of a prostate cancer patient with improved spatial resolution up to $0.35 \times 0.35 \times 2$ mm^3. It is shown for one patient that tumor-to-tissue contrast improves at 7T as compared with 3T. At 7T, increasing the resolution from $0.78 \times 0.78 \times 3$ mm^3 to $0.5 \times 0.5 \times 2$ mm^2 also improved tumor-to-tissue contrast for the same patient. A systematic comparison in more patients and using full prostate coverage is needed to draw any definite conclusions on image quality in T_2w imaging at 7T as compared with 3T. Not only T_2w imaging benefits from the higher SNR: MR spectroscopy, dynamic contrast-enhanced sequences, and diffusion-weighted imaging are only a few of the prostate cancer characterization methods that can also profit from a higher SNR, while some of these simultaneously profit from an enhanced contrast mechanism at higher field strengths that comes on top of the SNR gain.

This study focused on the comparison of system SNR values. To account for differences in system losses, the loaded to unloaded Q-factor ratio of the coils and the preamplifier noise figure can be used as a correction factor to obtain intrinsic SNR values.[23] However, for the commercial array it was not possible to measure the loaded-to-unloaded Q-factor ratio. A worst-case assumption based on literature values for very small loop coils in an array setup[36] would result in a correction factor of 0.79 for the 3T array. The high loaded-to-unloaded Q-factor ratio of the 7T array would result in a correction factor of 0.96.[29] According to this worst-case assumption, and including a correction factor for the preamplifier noise figure (0.93 at 3T and 0.91 at 7T), intrinsic SNR gain at 7T would be 1.9-fold instead of 2.2-fold.

Intrinsic SNR values are determined by the B_0 field strength but also by the receive sensitivities of the coil arrays. Different coil setups were used at 3T and 7T, which may be considered a source of bias even after correcting for loaded to unloaded Q-factor ratio. However, a 3T vs. 7T comparison with identical coils would favor one of the field strengths, as optimal coil design depends on the field strength. In this study, the 7T coil array was an in-house developed array that resulted from a gradual evolution of body imaging arrays at 7T.[21,22,30] The 3T coil array is a widely used, state-of-the-art commercial coil and it is also the coil array that is used for prostate cancer patients in our department. It is therefore considered an appropriate reference. Nevertheless, it is not impossible that for both field strengths the SNR may be improved by adapted coil array designs. The use of endorectal coils, which can further increase SNR at the cost of subject discomfort, is not treated in this article. Endorectal coils for 7T prostate imaging have been used.[16,18,19] As the results in this study show, SNR is gained at 7T compared with 3T, especially in regions closer to the coil. This may indicate that SNR gains at 7T are even larger compared with 3T when adding an endorectal coil at both field strengths. However, since an endorectal coil was not used in this study, this remains to be shown in practice.

The main aim of this work was to demonstrate the gain in intrinsic SNR for prostate imaging at 7T in comparison to 3T. The results show that the additional signal at 7T outweighs the reduced penetration depth of the RF signals. Although the gain in intrinsic SNR is clear, the exact quantitative outcome (1.7 up to 2.8-fold increase) bears some uncertainty related to the limited number of subjects included in the study. Also, we would like to emphasize that the patient data shown in this work merely serves as an example of what clinical 7T imaging with this intrinsic SNR level may achieve. A more extensive clinical study is needed to investigate to what extent the increase in intrinsic SNR translates into better imaging performance for clinically relevant sequences, which will be influenced by differences in T_1, T_2, SAR constraints, and potentially also the likelihood of image artifacts. Note that particularly the SAR constraints are still subject to improvement. The current study used conservative settings of maximum 4W per channel that are based on large overestimations. Current research activity is focused on safely reducing these overestimations.[31,40] A clinical comparison study should preferably be performed after optimization of our SAR safety assessment protocol that is currently based on many worst-case assumptions resulting in overly constrained sequences.

In conclusion, this study shows a comparison of SNR for prostate imaging at 7T and 3T. Compared with a clinically used prostate imaging setup at 3T, 7T imaging resulted in an SNR gain ranging from 1.7-fold to 2.8-fold. An LR acceleration factor R = 4 can be applied at 7T to acquire an image with comparable SNR to an unaccelerated 3T image. Furthermore, T_2w imaging was done at 3T and 7T in one patient, where improved tumor-to-tissue contrast was demonstrated at 7T.

References

1. Siegel RL, Miller KD, Jemal A. Cancer statistics, 2017. CA Cancer J Clin 2017;67:7–30.

2. Draisma G, Boer R, Otto SJ, et al. Lead times and overdetection due to prostate-specific antigen screening: estimates from the European Randomized Study of Screening for Prostate Cancer. J Natl Cancer Inst 2003;95:868–878.

3. Shukla-Dave A, Hricak H. Role of MRI in prostate cancer detection. NMR Biomed 2014;27:16–24.

4. Nagarajan R, Margolis D, Raman S, et al. MR spectroscopic imaging and diffusion-weighted imaging of prostate cancer with Gleason scores. J Magn Reson Imaging 2012;36:697–703 http://www.ncbi.nlm.nih.gov/pubmed/22581787.

5. Tempany C, Franco F. Prostate MRI: Update and current roles. Appl Radiol 2012;41:17–22.
6. Scheenen TWJ, Rosenkrantz AB, Haider MA, Fütterer JJ. Multiparametric magnetic resonance imaging in prostate cancer management: Current status and future perspectives. Invest Radiol 2015;50:594–600.
7. Turkbey B, Brown AM, Sankineni S, Wood BJ, Pinto PA, Choyke PL. Multiparametric prostate magnetic resonance imaging in the evaluation of prostate cancer. CA Cancer J Clin 2016;66:326–336.
8. Kobus T, Hambrock T, Hulsbergen-Van De Kaa CA, et al. In vivo assessment of prostate cancer aggressiveness using magnetic resonance spectroscopic imaging at 3 T with an endorectal coil. Eur Urol 2011;60: 1074–1080.
9. Kurth J, Defeo E, Cheng LL. Magnetic resonance spectroscopy: a promising tool for the diagnostics of human prostate cancer? Urol Oncol 2011; 29:562–571 http://www.ncbi.nlm.nih.gov/pubmed/21930088.
10. Vos EK, Kobus T, Litjens GJS, et al. Multiparametric magnetic resonance imaging for discriminating low-grade from high-grade prostate cancer. Invest Radiol 2015;50:490–497.
11. Fütterer JJ. High-resolution diffusion-weighted imaging increases prostate cancer visibility? EBioMedicine 2016. p 12.
12. Cornfeld DM, Weinreb JC. MR imaging of the prostate: 1.5T versus 3T. Magn Reson Imaging Clin N Am 2007:433–448.
13. Laader A, Beiderwellen K, Kraff O, et al. 1.5 versus 3 versus 7 Tesla in abdominal MRI: A comparative study. PLoS One 2017;12:e0187528.
14. Vos EK, Lagemaat MW, Barentsz JO, et al. Image quality and cancer visibility of T2-weighted magnetic resonance imaging of the prostate at 7 Tesla. Eur Radiol 2014;24:1950–1958.
15. Lagemaat MW, Vos EK, Maas MC, et al. Phosphorus magnetic resonance spectroscopic imaging at 7 T in patients with prostate cancer. Invest Radiol 2014;49:363–372.
16. Luttje MP, Italiaander MGM, Arteaga de Castro CS, et al. (31) P MR spectroscopic imaging combined with (1) H MR spectroscopic imaging in the human prostate using a double tuned endorectal coil at 7T. Magn Reson Med 2014;72:1516–1521 http://www.ncbi.nlm.nih.gov/pubmed/24357271.
17. Arteaga de Castro CS, Luttje MP, Van Vulpen M, Luijten PR, Van der Heide UA, Klomp DWJ. Composite slice-selective adiabatic excitation for prostate MRSI. NMR Biomed 2013;26:436–442.
18. Metzger GJ, Van De Moortele PF, Akgun C, et al. Performance of external and internal coil configurations for prostate investigations at 7 T. Magn Reson Med 2010;64:1625–1639.
19. Maas MC, Vos EK, Lagemaat MW, et al. Feasibility of T2-weighted turbo spin echo imaging of the human prostate at 7 Tesla. Magn Reson Med 2014;71:1711–1719 http://www.ncbi.nlm.nih.gov/pubmed/23798333.
20. Raaijmakers AJE, Ipek O, Klomp DWJ, et al. Design of a radiative surface coil array element at 7 T: The single-side adapted dipole antenna. Magn Reson Med Wiley Online Library; 2011;66:1488–1497.
21. Raaijmakers AJE, Italiaander M, Voogt IJ, et al. The fractionated dipole antenna: A new antenna for body imaging at 7 Tesla. Magn Reson Med 2016;75:1366–1374 http://dx.doi.org/10.1002/mrm.25596.
22. Rosenkrantz AB, Zhang B, Ben-Eliezer N, et al. T2-weighted prostate MRI at 7 Tesla using a simplified external transmit-receive coil array: Correlation with radical prostatectomy findings in two prostate cancer patients. J Magn Reson Imaging 2015;41:226–232.
23. Edelstein WA, Glover GH, Hardy CJ, Redington RW. The intrinsic signal-to-noise ratio in NMR imaging. Magn Reson Med 1986;3:604–618.
24. Roemer PB, Edelstein WA, Hayes CE, Souza SP, Mueller OM. The NMR phased array. Magn Reson Med 1990;16:192–225.
25. Vaughan JT, Garwood M, Collins CM, et al. 7T vs. 4T: RF power, homogeneity, and signal-to-noise comparison in head images. Magn Reson Med Wiley Online Library; 2001;46:24–30.
26. Kellman P, McVeigh ER. Image reconstruction in SNR units: A general method for SNR measurement. Magn Reson Med 2005;54:1439–1447.
27. Kellman P. Erratum to Kellman P, McVeigh ER. Image reconstruction in SNR units: a general method for SNR measurement. Magn Reson Med 2007;58:211–212.
28. Wiesinger F, Boesiger P, Pruessmann KP. Electrodynamics and ultimate SNR in parallel MR imaging. Magn Reson Med Wiley Online Library; 2004;52:376–390.
29. Steensma BR, Voogt IJ, Leiner T, et al. An 8-channel Tx / Rx dipole array combined with 16 Rx loops for high – resolution functional cardiac imaging at 7 T. Magn Reson Mater Phys Biol Med Berlin Heidelberg: Springer; 2017;0123456789 https://doi.org/10.1007/s10334-017-0665-5.
30. Raaijmakers AJE, Luijten PR, van den Berg CAT. Dipole antennas for ultrahigh-field body imaging: a comparison with loop coils. NMR Biomed 2016;29:1122–1130.
31. Meliado EF, Raaijmakers AJE, Luijten PR, van den Berg CAT. Fast method to get an upper bound of the maximum SAR10g for body coil arrays. In: Proc 9th Sci Meet Int Soc Magn Reson Med Benelux Chapter, Tilbg. 2017;p-070.
32. Metzger GJ, Snyder C, Akgun C, Vaughan T, Ugurbil K, Van De Moortele PF. Local B1 + shimming for prostate imaging with transceiver arrays at 7T based on subject-dependent transmit phase measurements. Magn Reson Med 2008;59:396–409.
33. Yarnykh VL. Actual flip-angle imaging in the pulsed steady state: A method for rapid three-dimensional mapping of the transmitted radiofrequency field. Magn Reson Med Wiley Subscription Services 2007;57: 192–200 http://dx.doi.org/10.1002/mrm.21120.
34. Heverhagen JT. Noise measurement and estimation in MR imaging experiments. Radiology 2007;245:638–639.
35. Roemer PB, Edelstein WA, Hayes CE, Souza SP, Mueller OM. The NMR phased array. Magn Reson Med. Wiley Subscription Services 1990;16: 192–225.
36. Kumar A, Edelstein WA, Bottomley PA. Noise figure limits for circular loop MR coils. Magn Reson Med 2009;61:1201–1209.
37. Chen G, Collins CM, Sodickson DK, Wiggins GC. A method to assess the loss of a dipole antenna for ultra-high-field MRI. Magn Reson Med 2018; 79:1773–1780.
38. Pruessmann KP, Weiger M, Scheidegger MB, Boesiger P. SENSE: Sensitivity encoding for fast MRI. Magn Reson Med 1999;42:952–962.
39. Ertürk MA, Raaijmakers AJE, Adriany G, Ugurbil K, Metzger GJ. A 16-channel combined loop-dipole transceiver array for 7 Tesla body MRI. Magn Reson Med 2016;76:1–11.
40. Meliado EF, Raaijmakers AJE, Restivo M, Maspero M, Luijten PR, van den Berg CAT. Database construction for local SAR prediction: Preliminary assessment of the intra and inter subject SAR variability in pelvic region. In: Proc 24th Annual Meeting ISMRM, Singapore; 2016. 3660.